Supplemental Material: Mott domain walls: a (strongly) non-Fermi liquid state of matter

Tsung-Han Lee,[1,2] J. Vučičević,[3] D. Tanasković,[3] E. Miranda,[4] and V. Dobrosavljević[1]

[1]*Department of Physics and National High Magnetic Field Laboratory, Florida State University, Tallahassee, Florida 32306, USA*

[2]*Physics and Astronomy Department, Rutgers University, Piscataway, New Jersey 08854, USA*

[3]*Institute of Physics Belgrade, University of Belgrade, Pregrevica 118, 11080 Belgrade, Serbia*

[4]*Gleb Wataghin Physics Institute, The University of Campinas, Rua Sérgio Buarque de Holanda, 777, CEP 13083-859, Campinas, Brazil*

In this Supplemental Material, we review, in Sec. I, the Ginzburg-Landau theory and the ϕ^4 theory for dynamical mean-field theory (DMFT) following Refs. [1–3] and the domain-wall solutions in the inhomogeneous Ginzburg-Landau theory. In Sec. II, we provide a detailed comparison of different analytic continuation results for the quasiparticle parameters and transport properties.

I. GINZBURG-LANDAU THEORY FOR DYNAMICAL MEAN-FIELD THEORY

We start from the Ginzburg-Landau free energy functional for DMFT [1]

$$F_{\mathrm{GL}}\big[G\big] = F_{\mathrm{imp}}\big[G\big] - \frac{t^2 T}{2}\sum_n G^2(i\omega_n). \tag{1}$$

Then, we expand the free energy functional around the critical point $\delta G = G - G_{\mathrm{cr}}$ leading to

$$F_{\mathrm{GL}} = F_{\mathrm{GL}}^{(0)} + F_{\mathrm{GL}}^{(1)} + F_{\mathrm{GL}}^{(2)} + F_{\mathrm{GL}}^{(3)} + F_{\mathrm{GL}}^{(4)}, \tag{2}$$

where

$$F_{\mathrm{GL}}^{(0)} = F_{\mathrm{GL}}\big[G_{\mathrm{cr}}\big], \tag{3}$$

$$F_{\mathrm{GL}}^{(l)} = \frac{T}{l}\sum_{k_1,\ldots,k_l}\Gamma^{(l)}_{k_1,\ldots,k_l}\big[G_{\mathrm{cr}}\big]\prod_{j=1}^{l}\delta G_{k_j}, \tag{4}$$

$$\Gamma^{(l)}_{k_1,\ldots,k_l}\big[G\big] = \frac{1}{T}\frac{l}{l!}\Big(\prod_{j=1}^{l}\frac{\delta}{\delta G_{k_j}}\Big)F_{\mathrm{GL}}\big[G\big], \tag{5}$$

$k \equiv (\mathbf{k}, i\omega_n)$ is the momentum and frequency index, and $F_{\mathrm{GL}}^{(1)} = 0$ from the DMFT self-consistency condition.

A. ϕ^4-model for dynamical mean-field theory

The DMFT Ginzburg-Landau functional can be mapped to a ϕ^4-model around the critical point [2, 3]. We write

$$\sum_{k_2}\Gamma^{(2)}_{k_1k_2}\big[G_{\mathrm{cr}}\big]\Psi_{\lambda,k_2p} = \Psi_{\lambda,pk_1}\gamma^{(2)}_{\lambda,p}, \tag{6}$$

where Ψ_{λ,k_1p} and $\gamma^{(2)}_{\lambda,p}$ is the eigenbasis and the eigenvalues of $\Gamma^{(2)}_{k_1k_2}$, respectively, and λ labels the eigenmodes. We then introduce the $\phi_{\lambda,p}$ defined by

$$\delta G_k = \sum_{\lambda,p}\Psi_{\lambda,kp}\phi_{\lambda,p}, \tag{7}$$

such that the Ginzburg-Landau free energy can be written in the eigenbasis as

$$F_{\rm GL}^{(2)} = \frac{T}{2}\sum_{P}\gamma_{P}^{(2)}|\phi_{P}|^{2} \tag{8}$$

$$F_{\rm GL}^{(3)} = \frac{T}{3}\sum_{P_1P_2P_3}\gamma_{P_1P_2P_3}^{(3)}\phi_{P_1}\phi_{P_2}\phi_{P_3} \tag{9}$$

$$F_{\rm GL}^{(4)} = \frac{T}{4}\sum_{P_1\ldots P_4}\gamma_{P_1P_2P_3P_4}^{(4)}\phi_{P_1}\phi_{P_2}\phi_{P_3}\phi_{P_4}, \tag{10}$$

where $P \equiv (\lambda, p)$ and

$$\gamma_{P_1\ldots P_l}^{(l)} = \sum_{k_1\ldots k_l}\Gamma_{k_1\ldots k_l}^{(l)}\big[G_{\rm cr}\big]\prod_{j=1}^{l}\Psi_{\lambda_j,k_jp_j}. \tag{11}$$

As pointed out in Refs. [1–3], the critical behavior is dominated by the soft eigenmode so we can project the free energy functional to this specific eigenbasis. Focusing on the static and uniform part of the free energy function, we can write down the ϕ^4-model for DMFT

$$\frac{F_{\rm GL}}{T} = \frac{1}{2}\sum_{p}\gamma^{(2)}\phi_p^2 + \frac{1}{3}\sum_{p_1p_2p_3}\gamma^{(3)}\phi_{p_1}\phi_{p_2}\phi_{p_3} + \frac{1}{4}\sum_{p_1p_2p_3p_4}\gamma^{(4)}\phi_{p_1}\phi_{p_2}\phi_{p_3}\phi_{p_4}. \tag{12}$$

B. Domain-wall solution

To interpret the domain-wall solution, we write the Ginzburg-Landau free energy in the real space

$$\frac{F_{\rm GL}\big[\phi\big]}{T} = \int d\mathbf{x}\Big\{\frac{\kappa}{2}\big(\nabla\phi(\mathbf{x})\big)^2 + \frac{1}{2}\gamma^{(2)}\phi(\mathbf{x})^2 + \frac{\gamma^{(4)}}{4}\phi(\mathbf{x})^4\Big\}, \tag{13}$$

where the cubic term in Eq. 12 can be eliminated by properly shifting the field ϕ [2, 3]. The Euler-Lagrange equation of $F_{\rm GL}$ is

$$\gamma^{(2)}\phi(\mathbf{x}) + \gamma^{(4)}\phi(\mathbf{x})^3 - \kappa\nabla^2\phi(\mathbf{x}) = 0. \tag{14}$$

For simplicity we consider the domain-wall forms along the x-direction, so the Euler-Lagrange equation becomes

$$\gamma^{(2)}\phi(x) + \gamma^{(4)}\phi(x)^3 - \kappa\phi''(x) = 0. \tag{15}$$

with the boundary condition $\phi(x\to-\infty) = -\phi_0$ and $\phi(x\to\infty) = \phi_0$ and $\phi_0 = \sqrt{-\gamma^{(2)}/\gamma^{(4)}}$. Note that the uniform saddle-point solution ϕ_0 can be related to the double occupancy or the density of states at the Fermi level, where the positive and negative values of ϕ_0 correspond to the metallic and the insulating solutions, respectively [2]. One can show that the inhomogeneous domain-wall solution is [4]

$$\phi(x) = \phi_0\tanh\big[\frac{x}{\sqrt{2}\xi}\big], \tag{16}$$

where $\xi = \sqrt{-\kappa/\gamma^{(2)}}$ is the correlation length. We can see that the domain-wall solution at $\phi(x) = 0$ corresponds to the local maximum of the uniform Landau free energy

$$f[\phi] = \frac{1}{2}\gamma^{(2)}\phi^2 + \frac{\gamma^{(4)}}{4}\phi^4 \tag{17}$$

shown schematically in Fig. 1.

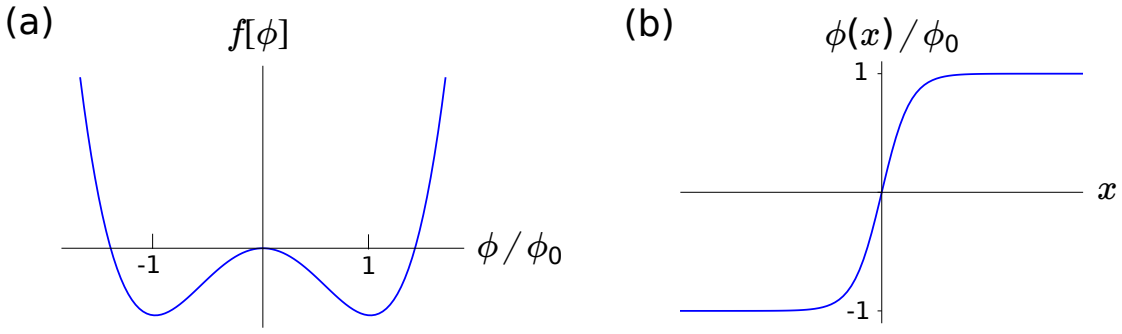

FIG. 1. (a) Schematic Landau free energy $f[\phi]$ as a function of ϕ. (b) Schematic domain-wall solution profile $\phi(x)$ as a function of x.

II. COMPARISON OF MAXIMUM ENTROPY METHOD AND POLYNOMIAL FITTING ANALYTIC CONTINUATION

In this section, we compare the quasiparticle and transport properties obtained from two analytic continuation approaches: maximum entropy method (MEM) and fifth-order polynomial fitting.

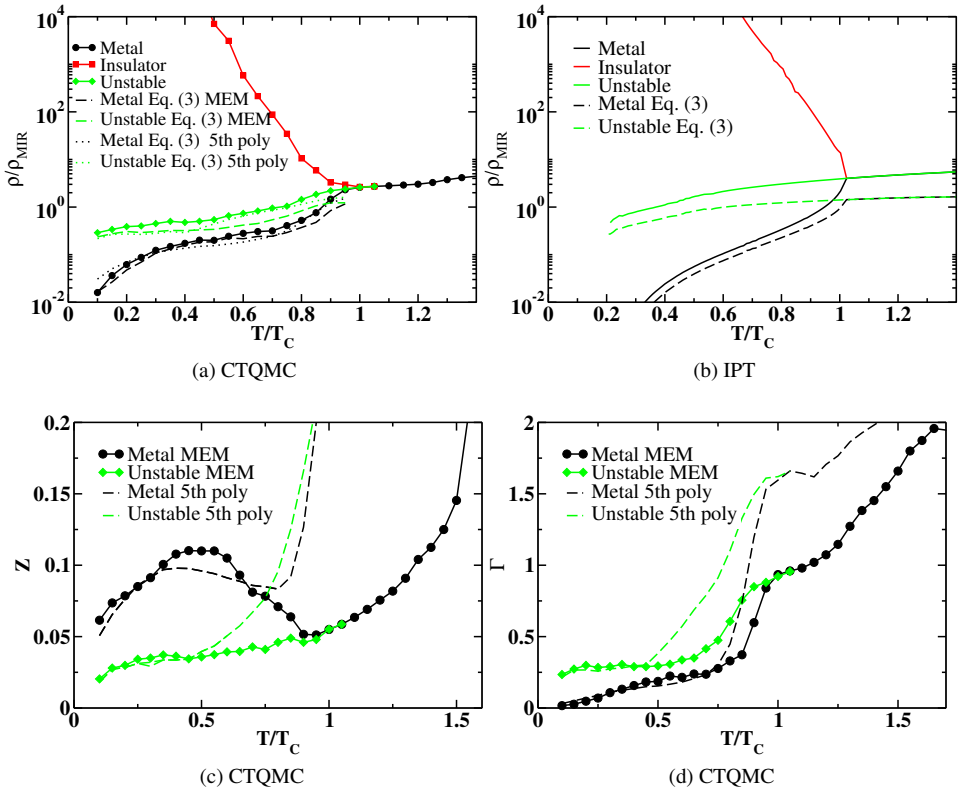

FIG. 2. The resistivity for the metallic (black circles), insulating (red squares), and unstable (green squares) solutions along the first-order transition line in a logarithmic ρ scale for (a) CTQMC and (b) IPT. The Sommerfeld approximations to the resistivities (Eq. (3)) are shown in the corresponding dashed and dotted lines with different analytic continuation methods (MEM and polynomial fitting for CTQMC and Padé approximation for IPT). (c) The quasiparticle weight, Z, for the metallic and unstable solutions analytic continued by MEM (black and green symbols) and by polynomial fitting (black and green dashed lines). (d) The scattering rate Γ, for the metallic and the unstable solutions, obtained from MEM (black and green symbols) and from polynomial fitting (black and green dashed lines).

First, we discuss the results along the first-order transition line. Figure 2(a) shows the resistivities computed from the Som-

merfeld approximation (Eq. (3) in the main text) using MEM and polynomial fitting analytic continuations. We see that the two analytic continuations agree at low temperatures. However, around T_c, the two methods show significant differences. This behavior is also observed in the quasiparticle weight Z (Fig. 2(c)) and the scattering rate Γ ((Fig. 2(d)). The difference between the two analytic continuation methods stems from the breakdown of the polynomial fitting around T_c, where the polynomial fitting of the first few Matsubara points of the self-energy does not yield reliable quasiparticle parameters Z and Γ. Therefore, around T_c, one should trust the MEM results. On the other hand, the polynomial fitting should be more reliable at low temperatures, where the first few Matsubara points are enough to determine the quasiparticle parameters, whereas the MEM is noisier.

We now discuss the results of different analytic continuation approaches along a constant U trajectory. In Fig. 3(a), we show the resistivity calculated from the Sommerfeld approximation (Eq. (3) in the main text) using MEM and polynomial fitting analytic continuation. We observe that the two analytic continuation approaches give semi-quantitatively similar behavior. In Fig. 3(c), we show the quasiparticle weight Z calculated from the two analytic continuation approaches. We observe that the two analytic continuations give the same behavior for the metallic solutions quantitatively. Note that the polynomial fitting is expected to give a more reliable analytic continued Z at low temperature. On the other hand, for the unstable solutions, we see that the two analytic continuation approaches yield different powers where the polynomial fitting gives $Z \sim T^{1.5}$ and MEM gives $Z \sim T^2$. Both differ significantly from the Fermi-liquid saturation behavior shown in the metallic solutions. Finally, in Fig. 3(d), we show the scattering rate Γ calculated from the two analytic continuation approaches. We observed that the two approaches give semi-quantitatively the same behavior with similar power, $\Gamma \sim T^2$ for the metallic solutions and $\Gamma \sim T^{-2}$ for the unstable solutions. We note that the polynomial fitting is expected to yield more reliable analytic continued Γ for the metallic solutions at low temperatures.

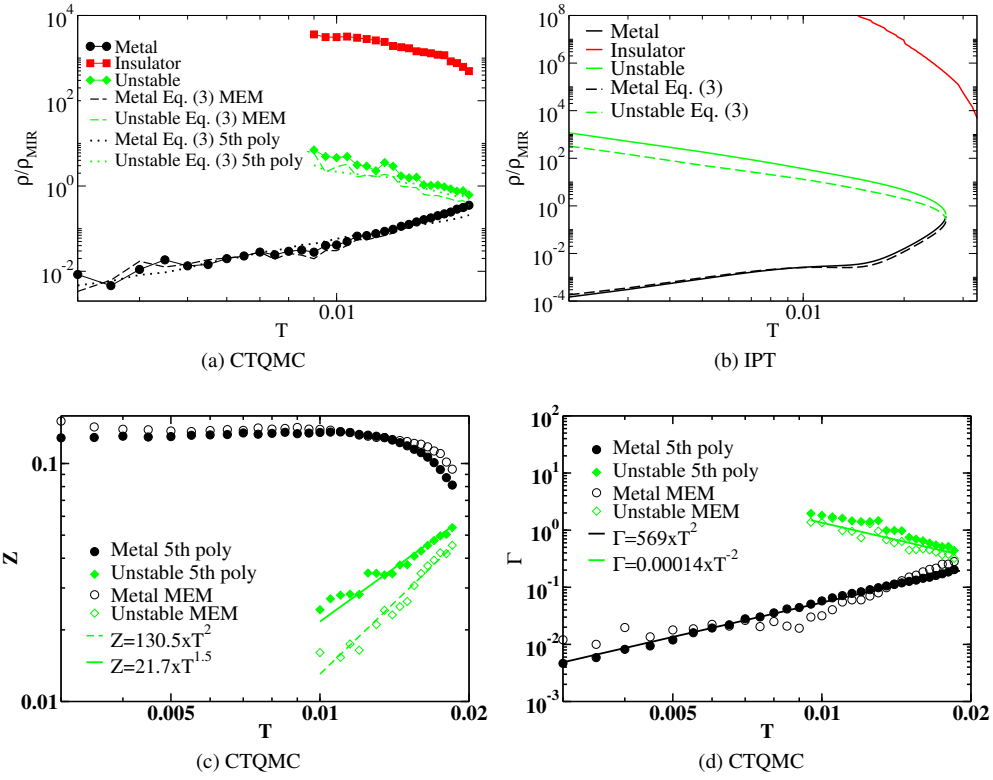

FIG. 3. The resistivity for the metallic (black circles), insulating (red squares), and unstable (green diamonds) solutions along the constant U trajectory in logarithmic ρ scale for (a) CTQMC and (b) IPT. The Sommerfeld approximations to the resistivities are shown in the corresponding dashed and dotted lines with different analytic continuation methods (MEM and polynomial fitting for CTQMC and Padé approximation for IPT). (c) The quasiparticle weight, Z, for the metallic and the unstable solutions. (d) The scattering rate Γ for the metallic and the unstable solutions.

REFERENCES

[1] Kotliar, G., Eur. Phys. J. B **11**, 27 (1999), URL https://doi.org/10.1007/s100510050914.

[2] G. Kotliar, E. Lange, and M. J. Rozenberg, Phys. Rev. Lett. **84**, 5180 (2000), URL https://link.aps.org/doi/10.1103/PhysRevLett.84.5180.

[3] S. Onoda (2004), URL https://arxiv.org/abs/cond-mat/0408207.

[4] P. M. Chaikin and T. C. Lubensky, *Principles of Condensed Matter Physics* (Cambridge University Press, 1995).